Biomass Conversion and Biorefinery (2023) 13:17101–17118
https://doi.org/10.1007/s13399-022-02372-w

ORIGINAL ARTICLE

Production of magnetic sewage sludge biochar: investigation of the activation mechanism and effect of the activating agent and temperature

Irene Sierra[1] · Unai Iriarte-Velasco[1] · Jose L. Ayastuy[2] · Andrés T. Aguayo[2]

Received: 20 September 2021 / Revised: 30 December 2021 / Accepted: 18 January 2022 / Published online: 11 February 2022

Abstract

Sewage sludge-based porous materials were prepared through an integrated and energy-saving procedure that combines chemical activation with an alkali (NaOH or K_2CO_3) and physical activation with CO_2 in a single step. The study was conducted in a wide temperature range (600–1000 °C), using higher temperatures than those commonly used. From the standpoint of textural properties, the impregnation results in a decrease in the optimum activation temperature: 800 °C for untreated samples, and 600–700 °C for impregnated samples. The impregnation increases the amount of –OH and –NH functional groups, and it also leads to the generation of new oxygen- and/or nitrogen-containing functionalities (above 800 °C for the impregnation with K_2CO_3 and in the whole temperature range for the impregnation with NaOH). The chemical treatment favors the development of magnetic properties on biochars, which is an advantage for its reuse in wastewater treatment, since it favors the removal of anionic surfactants and heavy metals such as lead, copper, zinc, and manganese. The uptake of phenol and methylene blue (MB) is maximized with the combination of the impregnation (with NaOH for phenol and K_2CO_3 for MB) and the use of a moderate temperature (600–700 °C). The optimum uptake values represent an increase of 87% and 152% for MB and phenol, respectively, compared to the highest value of non-impregnated samples (activated at 800 °C), with the advantage of the lower temperature required.

Keywords Sewage sludge · Carbon dioxide · Alkali activation · Phenol · Methylene blue · Biochar

1 Introduction

The amount of sewage sludge is increasing due to population growth, urbanization, and industrial development, and more stringent standards for the discharge of wastewater to aquatic bodies. Sewage sludge is mainly composed of substances responsible for the toxic and pathogenic nature of non-treated wastewater and, therefore, its management is an issue of particular concern. Sewage sludge is a heterogeneous mixture of water, organic matter, microorganisms, and inorganic substances. The amount of the inorganic fraction is usually higher than 50 wt% [1]. Dry sewage sludge contains nitrogen and phosphorus in different forms. Sludge also contains high concentrations of inorganic salts including ions (CO_3^{2-}, PO_4^{3-}, SO_4^{2-}, and NO_3^-), heavy metals (e.g., Zn, Pb, Ni, Cd, Cr, Cu, As, and Hg), and other elements (e.g., Si, Al, K, Na, Ca, and Mg) [2]. The composition of sewage sludge is highly variable, since it is affected by different parameters such as the specificity of the sludge source

Highlights
- Sewage sludge-based porous materials were prepared through an integrated procedure.
- The preparation method combines alkali and physical activation with CO_2 in one step.
- Impregnation increases –OH/–NH functional groups and generates new functionalities.
- The alkali treatment favors the development of magnetic properties on biochars.
- Cost-effective biochars for MB and phenol removal were prepared at 600 °C.

✉ Irene Sierra
irene.sierra@ehu.eus

[1] Department of Chemical Engineering, Faculty of Pharmacy, University of the Basque Country (UPV/EHU), Vitoria-Gasteiz, Spain

[2] Department of Chemical Engineering, Faculty of Science and Technology, University of the Basque Country (UPV/EHU), Leioa, Spain

area, the processes carried out in the wastewater treatment plant, and the season [3].

Common routes of utilization and disposal, including land filling, application to farmland, and forestry and incineration, have serious limitations because of increasing costs and more stringent environmental standards to avoid secondary pollution [4]. Among the alternatives, the production of adsorbents is a promising way because, apart from being an eco-friendly alternative for the valorisation of sludge, it has the advantage of allowing its reuse in water treatment.

An increasing number of studies have been recently conducted to convert sewage sludge into adsorbents [5–11]. The activation procedure comprises several steps which initiate with drying of wet sewage sludge, with the aim of minimizing the requirement of energy for the subsequent thermal treatment [12]. The subsequent activation procedure can be either chemical or physical. In chemical activation, the precursor (either sewage sludge or pre-carbonized sludge) is mixed with a reagent, such as H_3PO_4 [13, 14], H_2SO_4 [15, 16], NaOH [17, 18], KOH [17, 19, 20], K_2CO_3 [14, 15], or $ZnCl_2$ [21, 22] and then heated up to a high temperature under an inert atmosphere. Physical activation is usually carried out through a two-step process. The first step involves the pre-carbonization of the precursor at a moderate temperature (400–700 °C) to break down the cross-linkage between carbon atoms [23]. The second stage comprises the selective burn-off of atoms from the carbonaceous structure by using gasifying agents such as steam [24, 25], air or oxygen [26, 27], and CO_2 [19, 28, 29] at high temperature. A post-activation washing of biochar with acids can generally remove the activation reagent residue and extraneous reaction products from the new free interstices formed, and reduce the inorganic content of the carbonaceous material [30]. In the current research, HF and HCl are the most used acids for sewage sludge–derived biochar [31]. The deashing of biochar by acid washing results in the opening of the pore channels; thus, the specific surface area and pore structure are greatly improved [32]. However, the removal of minerals also leads to a reduction of the biochar production yield of about 50% [33, 34].

An alternative to the physical or chemical activation is the use of combined multiple activation methods, an issue not sufficiently investigated in the production of sludge biochar [2]. In the preparation procedure used in this study, both chemical and physical activation processes are integrated in a single step. The preparation method takes advantage of the heating step of the chemical activation to introduce an oxidizing gas (CO_2, in this case), instead of an inert atmosphere. Compared to the chemical activation, it has the potential to further improve the textural properties and the adsorption capacities of the biochars [35] without adding a new heating step.

The combined activation in one step has been reported to have a significant impact both on the porosity and on surface functional groups of materials prepared from carbonaceous precursors such as agricultural wastes [36, 37]. Nevertheless, it has been scarcely studied for sewage sludge. Wang et al. [38] studied the combined activation of sewage sludge with KOH and steam, and more recently, the activation of sewage sludge with HCl under CO_2 atmosphere has been investigated [28, 33]. Nevertheless, to the best of the author's knowledge, there are no reports concerning the combined activation of alkali-treated samples of sewage sludge under CO_2 atmosphere.

The objective of the present paper is to investigate the preparation of porous biochars through a procedure that combines chemical activation with an alkali (NaOH or K_2CO_3) and physical activation with CO_2 in a single step. The contribution of this work can be summarized as follows: (i) Utilization of a promising and sustainable combined activation method, not reported in the literature for the preparation of sludge-based biochar. The sustainability is based on the utilization of CO_2 as oxidizing gas and on the absence of a pre-carbonization step, thus leading to an important reduction of the preparation cost, due to energy saving, higher yield of biochar, lower capital and operational costs, and less processing time [37]. (ii) Study of a wide activation temperature range (600–1000 °C), including higher temperatures than those commonly reported in the literature, to ensure an effective activation using CO_2, based on its low reactivity, due to its large molecular size [37] and the endothermicity of its reaction with carbon [4]. (iii) Proposal of an activation mechanism that takes into account the effect of each activating agent. (iv) Investigation of the application of the biochars in the removal of aqueous pollutants using two model compounds, methylene blue and phenol.

2 Materials and methods

2.1 Raw material

Anaerobically digested and dewatered sewage sludge was collected from an urban wastewater plant. Raw sludge was dried at 105 °C for 48 h in a convection oven. According to the proximate analysis of the material, its high water content (73.3 wt%) is noteworthy. Dried sewage sludge has a similar percentage of ash and volatile matter (42.2 wt% and 49.2 wt%, respectively), and the content of fixed carbon is relatively low (8.6 wt%).

Table 1 shows the results of the elemental analysis and the concentration of heavy metals corresponding to the feedstock used in this study. As it generally occurs, carbon is the most abundant element. Carbon can be present in organic compounds (e.g., aliphatic and aromatic hydrocarbons) and

Table 1 Results of elemental analysis and concentration of heavy metals of sewage sludge. Elemental analysis, wt%. Heavy metals, mg/kg

Sample	C	H	N	Cr	Ni	Cu	Zn	Pd
Sewage sludge	29.7	4.1	3.2	167	586	376	3123	< 0.02

inorganic compounds (such as carbonates) [39]. Hydrogen mainly includes aromatic hydrogen, fatty hydrogen, and hydrogen in functional groups [40]. Nitrogen is mainly present in proteins in biomass [41]. Oxygen can also take part of organic constituents (e.g., hydroxyl, carboxyl, and carbonyl) and inorganic constituents (e.g., bicarbonate, carbonate, and phosphate) [41].

2.2 Preparation of sludge carbon

Dried sewage sludge was ground with a mortar and sieved. Particles within the 0.5–1.0 mm size range were selected. The impregnation ratio was established at 60 mmol activation agent/$g_{precursor}$ (dried sewage sludge), which is within the normal range used for the chemical activation of sewage sludge [14, 42, 43] and ensures sufficient interaction between the activation agent and the precursor. To carry out the impregnation, about 1 g of sewage sludge was added to 20 cm^3 of a 3 M solution containing the activating agent (NaOH or K_2CO_3).

The solutions were introduced in 50 cm^3 borosilicate amber glass vials and maintained under constant stirring at 150 rpm in a reciprocating shaker at room temperature (20 ± 2 °C) for 48 h, to ensure the access of the agent to the interior of the particles. Samples were then filtered, transferred to a convection oven, and dried at 80 °C for 24 h. A part of the precursor, used as reference, was not impregnated.

The thermal treatment (conventional slow pyrolysis) was conducted in a quartz tube furnace, under CO_2 atmosphere (120 cm^3/min of flowing gas, corresponding to 8 min of residence time). The impregnated sludge was heated from room temperature to 600–1000 °C, using a low heating rate of 15 °C/min. Samples were soaked at the final temperature for 30 min, and then cooled down in nitrogen atmosphere. The obtained biochars were washed with distilled water until a neutral pH was reached.

The samples of sludge carbon (SC) prepared by physical activation only were coded based on the temperature: SC-600, SC-700, SC-800, SC-900, and SC-1000. The samples subjected to a combined physical and chemical activation process were coded based on the activation reagent—NaOH (SCN) or K_2CO_3 (SCK)—and temperature. For instance, SCN-600 refers to sludge carbon impregnated with NaOH and activated in CO_2 atmosphere at 600 °C.

2.3 Characterization

The precursor (dried sewage sludge) was subjected to elemental analysis using CHNS analyzer (Euro-Vector EA-3000). The total concentration of heavy metals (Cr, Ni, Cu, Zn, and Pd) in the precursor was determined by a high-performance inductively coupled plasma mass spectrometer (ICP-MS, 7500ce Agilent Technologies). Prior to heavy metal determination, samples were microwave digested (Speedwave Four, Berghof) using an acid mixture (HNO_3:HF = 3:1).

The precursor and samples impregnated with NaOH and K_2CO_3 were subjected to thermogravimetric analysis (TG) in a thermobalance (T.A. Instruments SDT 2960), under inert (nitrogen) atmosphere. The alumina crucible of the thermobalance was loaded with 15–20 mg of sample, and subjected to heating from room temperature to 800 °C, using a heating rate of 10 °C/min. The textural properties of sludge biochar were determined by N_2 adsorption/desorption at 77 K (ASAP 2010, Micromeritics). Prior to measurements, samples were outgassed under N_2 flow at 200 °C for 15 h. Specific surface area was determined using the Brunauer–Emmett–Teller (BET) method. Surface area and pore volume in the mesopore and macropore range were obtained using the Barrett, Joyner, and Halenda (BJH) method, while values in the micropore range were calculated based on the t-plot method.

pH was determined following the method described by Tessmer et al. [44]. Ash content was measured by heating the samples under air atmosphere for 1 h at 815 °C (UNE 32004 standard). Fourier transform infrared (FTIR) measurements were carried out by means of a Thermo Nicolet 6700 equipment in the absorbance mode, using the KBr self-supported pellet technique. Spectra were collected in the 400–4000 cm^{-1} range with a resolution of 2 cm^{-1}. X-ray powder diffraction patterns were collected using a Philips X'pert PRO automatic diffractometer operating at 40 kV and 40 mA, in theta-theta configuration, secondary monochromator with Cu-Kα radiation (λ = 1.5418 Å) and a PIXcel solid state detector (active length in 2θ 3.347°). Data were collected from 5 to 90° 2θ (step size = 0.026 and time per step = 1000 s) at RT. A fixed divergence and antiscattering slit giving a constant volume of sample illumination were used. X-ray fluorescence (XRF) analysis was conducted using a Pananalytical AXIOS X-ray fluorescence spectrometer. Borate fusion was used to prepare sample beads, at a dilution ratio of 20:1.

Raman analysis was carried out in a Renishaw InVia Raman spectrometer coupled to a Leica DMLM microscope, using a laser of 514 nm (ion-argon laser, Modu-Laser). The power density of the laser beam was reduced in order to avoid the photo-decomposition of the samples. In order to improve the signal-to-noise ratio, 40 s was used for each spectrum and 10 scans were accumulated at 10% of the maximum power of the 514 nm laser, in the 1000–2000 cm^{-1} spectral window.

The chemical composition and surface properties of the materials were analyzed by a scanning electron microscope (JEOL JSM-7000F) equipped with an energy-dispersive X-ray (EDX) detector. Measurements were taken at a live time of 120 s with a voltage of 20 kV.

2.4 Adsorption experiments

Methylene blue (MB) and phenol were used as target adsorbates because they possess different physicochemical properties and molecular size. MB has a basic nature, and can be used as an indicator of the adsorption capacity in the micro- and mesopore range. Phenol has an acidic nature, and, owing to its smaller size, can be used as an indicator of micropores.

Single solute adsorption isotherms were obtained using the conventional bottle-point technique. Sludge carbon (10–15 mg) was contacted in stoppered glass bottles with 10 cm^3 of aqueous solutions with known concentration of MB or phenol. The flasks were shaken for 72 h by means of a rotary mixer placed in a thermostatic chamber at 20 °C ± 0.5 °C. The speed of the rotary mixer was set at 12 rpm. Preliminary tests revealed that a holding time of 72 h is enough to reach the equilibrium. After 72 h, samples were subjected to centrifugation, and the residual concentration of the solute in the supernatant was analyzed by UV/VIS spectrophotometry (Jasco V-630). The concentration of MB and phenol was obtained by collecting the UV absorbance at a wavelength of 662 and 270 nm, respectively. Blank runs (without sludge carbon) were carried out to take into account any effect of the experimental system.

The adsorption capacity of sludge carbon (q_e, mg/g) was determined by mass balance:

$$q_e = (C_0 - C_e)\, V/m \tag{1}$$

where C_0 and C_e are the initial and equilibrium concentrations of the adsorbate (mg/L), respectively. V is the solution volume (L) and m is the adsorbent mass (g).

Randomly selected experiments were carried out in triplicate, and the mean values were reported.

The adsorption isotherms of both adsorbates were determined, by fitting the equilibrium data to the Redlich-Peterson equation (Eq. 2):

$$q_e = \frac{K_R \cdot C_e}{1 + \alpha \cdot C_e^{\beta}} \tag{2}$$

where K_R is the Redlich-Peterson constant (L/g), α is a constant with units of $(L/mg)^{\beta}$, and β is an exponent between 0 and 1.

The best fitting parameters were calculated by non-linear regression. The goodness of fit between the experimental and predicted values was determined using the average percentage error (APE):

$$APE = \frac{\sum_{i=1}^{n} \left| (q_{e,exp} - q_{e,pred})/q_{e.\,exp} \right|}{n} \cdot 100 \tag{3}$$

where $q_{e,exp}$ is the experimental uptake capacity, $q_{e,pred}$ is the calculated uptake capacity, and n is the number of experiments.

3 Results and discussion

3.1 Characterization of raw sludge and investigation of the activation mechanism

The nature of raw sludge was analyzed elsewhere [33]. The results reveal that the precursor is an anaerobically digested and well-stabilized sewage sludge, with a low degree of polymerization and aromatization.

The weight loss of raw sewage sludge during the pyrolysis under nitrogen atmosphere can be divided into three main sections (Fig. 1), in good agreement with the profiles reported in the literature [45]. Nevertheless, the TG and DTG curves of municipal sewage sludge may have differences in shape, due to its complex composition [46]. The first stage (below 175 °C) could be attributed to moisture loss. The most important weight loss takes place at intermediate temperatures, between 175 and 550 °C. The processes involved in this stage include the release of constitution water and the decomposition and volatilization of organic matter [47, 48]. The DTG profile (Fig. 1b), similar to those reported by others [49, 50], shows two overlapping peaks with maxima around 290 and 330 °C, and a shoulder close to 450 °C. According to Xiaohua and Jiancheng [46], the peaks near 300 °C are related to the decomposition of aliphatic compounds, whereas the shoulder is attributed to the decomposition of carbohydrate and proteins. The final mass loss, at temperatures higher than 550 °C, is commonly attributed to the decomposition of minerals like calcium carbonate [45].

The samples impregnated with NaOH and K_2CO_3 exhibit different TG and DTG profiles (Fig. 1). The first stage of mass loss (below 175 °C), attributed to the evaporation of adsorbed water, is more pronounced, thus evidencing the

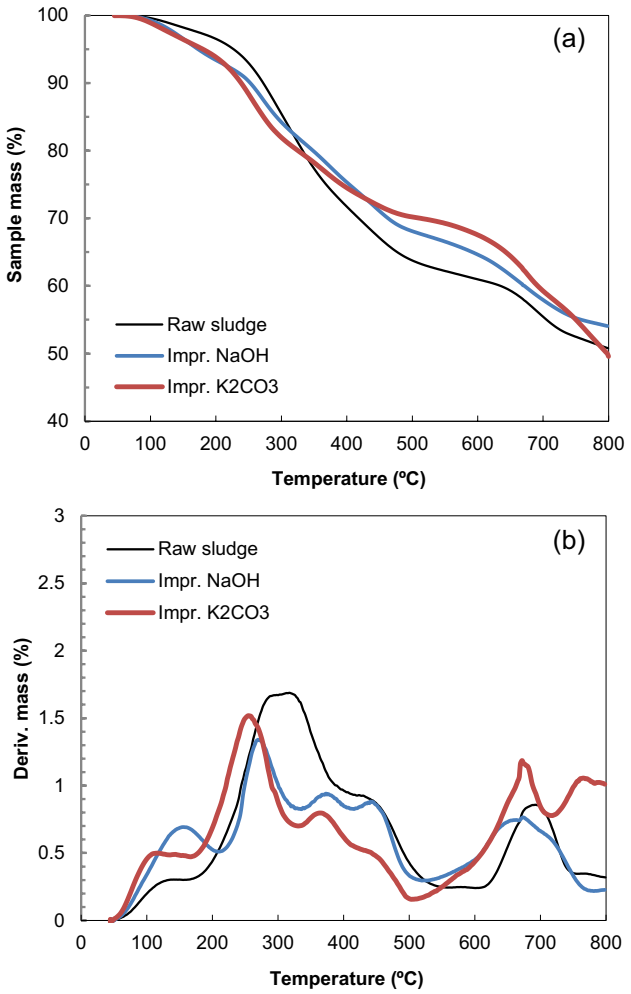

Fig. 1 Thermogravimetric results of raw sludge and sludge impregnated with NaOH and K_2CO_3 under inert (N_2) atmosphere. **a** TG curves; **b** DTG curves

hygroscopic nature of both reagents. The weight loss above 600 °C is higher for the sample impregnated with K_2CO_3, as expected, due partly to the thermal decomposition of the incorporated carbonates.

The weight loss at the intermediate temperature range (175–550 °C) shows important differences between raw sludge and impregnated samples. The peaks appear more clearly defined in the case of the impregnated samples. The peak at around 290 °C is shifted to lower temperature, thus evidencing the interaction between the precursor and the reagent. Furthermore, the impregnated samples lead to a lower weight loss at intermediate temperatures, which could be explained by the high amount of salts incorporated during the impregnation. According to the results of XRF analysis (Table 2), SCK samples possess a remarkable amount of K_2O (about 5 wt% vs. 0.3–0.8 wt% of the other samples), whereas SCN samples exhibit a remarkable Na_2O amount (11–12 wt% vs. 0.1–0.5 wt% of the other samples).

Table 2 Results of XRF analysis for selected samples of sludge biochar. Main elements, expressed as weight percentage of the oxide. Other elements, expressed as weight percentage of the element

	Main elements									Other elements		
Sample	SiO_2	Al_2O_3	Fe_2O_3*	MnO	MgO	CaO	Na_2O	K_2O	TiO_2	P_2O_5	Cu	S	Zn
SC-800	14.19	7.15	15.18	0.12	1.11	16.84	0.35	0.60	0.58	11.36	0.09	0.78	0.55
SC-900	18.54	8.91	19.88	0.14	1.33	19.71	0.48	0.85	0.75	14.93	0.24	1.07	0.64
SCK-800	14.51	6.88	14.71	0.11	1.08	19.62	0.24	5.31	0.61	9.43	0.10	0.62	0.53
SCK-900	14.35	7.62	16.38	0.12	1.14	22.30	0.10	4.83	0.68	10.75	0.11	1.68	0.34
SCN-800	14.00	5.63	19.34	0.16	1.19	21.54	10.74	0.64	0.65	11.49	0.12	0.31	0.56
SCN-900	14.85	5.54	18.80	0.14	1.16	22.21	11.99	0.27	0.69	10.73	0.11	0.81	0.59

*Iron content expressed as total Fe_2O_3

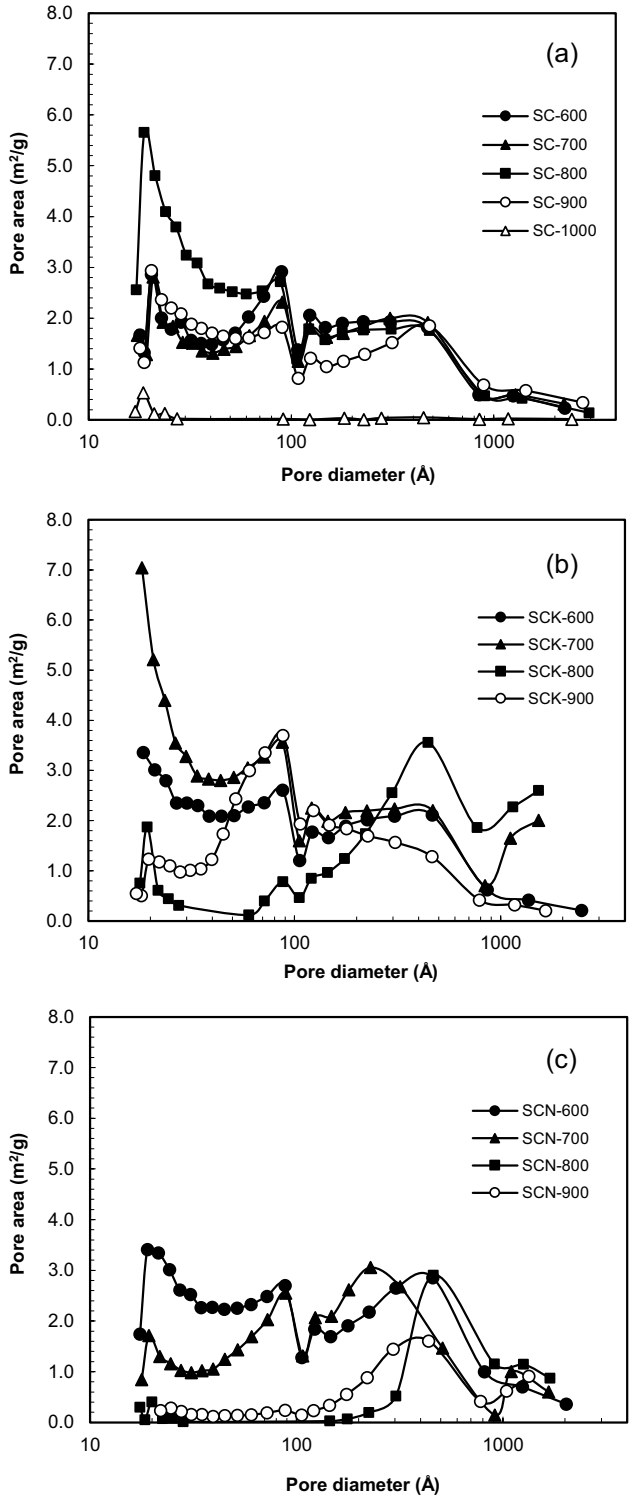

Fig. 2 Pore size distribution of samples of sludge carbon. **a** Samples prepared by physical activation with CO_2 only; **b** samples prepared by impregnation with K_2CO_3 followed by activation with CO_2; **c** samples prepared by impregnation with NaOH followed by activation with CO_2

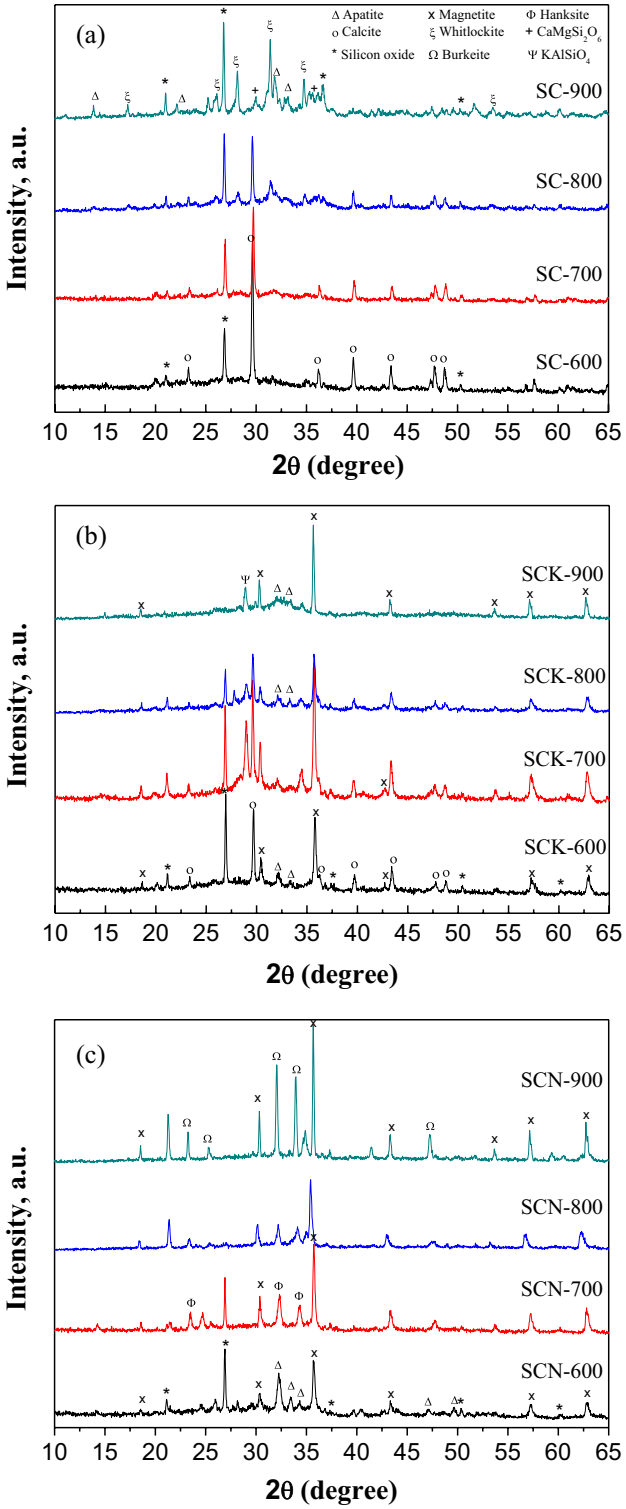

Fig. 3 XRD patterns of samples of sludge carbon. **a** Samples prepared by physical activation with CO_2 only; **b** samples prepared by impregnation with K_2CO_3 followed by activation with CO_2; **c** samples prepared by impregnation with NaOH followed by activation with CO_2

In our previous works, a preliminary study on the physical activation mechanism of raw sewage sludge with CO_2 was performed [28, 33]. Moreover, based on an extensive research concerning the chemical activation mechanism of a carbonaceous precursor using different reagents, including NaOH and K_2CO_3 [51], the following reactions and processes can be proposed for the activation with CO_2 of non-impregnated sludge: (i) the decomposition/volatilization of organic matter; (ii) the decomposition/volatilization of inorganic constituents, such as calcium carbonate; (iii) the desorption of water; (iv) the gasification of carbon through two reactions: the reverse Boudouard reaction (Eq. (4) and the reaction of carbon with steam (Eq. (5); (v) the water–gas shift reaction (Eq. (6); and (vi) the reaction of carbon and OH^-, to produce compounds such as cyanides, hydrocarbons, and carbonates, as discussed below. All these reactions are gasification reactions, except for Eq. (6), and, thus, are expected to generate porosity in the solid matrix.

$$C\ (s) + CO_2\ (g) \rightarrow 2\ CO\ (g) \tag{4}$$

$$C\ (s) + H_2O\ (g) \rightarrow H_2\ (g) + CO\ (g) \tag{5}$$

$$CO\ (g) + H_2O(g) \leftrightarrow H_2(g) + CO_2\ (g) \tag{6}$$

Two pathways have been proposed for the reaction of carbon constituent with OH^- ions. The first one results in the production of compounds such as cyanides and hydrocarbons. CN^- ions were detected during the activation of different carbonaceous precursors, including sewage sludge [28, 33, 51, 52]. Robau-Sánchez et al. [52] proposed several mechanisms for the activation with KOH of *Quercus agrifolia char* that leads to the formation of cyanides, such as Eq. (7):

$$6\ KOH\ (l) + 5.5\ C\ (s) + N_2\ (g) \rightarrow K_2\ (CN)_2\ (g) + 2\ K_2\ CO_3\ (s,l) + 1.5\ CH_4\ (g) \tag{7}$$

That mechanism that implies the reaction of carbon, nitrogen, and OH^- ions was proposed in our previous papers for non-impregnated carbonaceous precursors—bone char [51] and sewage sludge [28, 33]—and it was concluded that structural nitrogen (constituent of the precursor) takes part in the activation process. Moreover, FTIR analyses reveal the presence of OH^-, as discussed below.

The second reaction pathway between OH^- ions and carbon was proposed by Lillo-Ródenas et al. [53, 54] during the chemical activation of anthracites with hydroxides:

$$6\ NaOH\ (s,l) + C\ (s) \rightarrow 2\ Na\ (s) + 3\ H_2\ (g) + 2\ Na_2CO_3\ (s,l) \tag{8}$$

Regarding the samples impregnated before the treatment with CO_2, the occurrence of additional processes or the intensification of the aforementioned processes could be expected. In the activation mechanism proposed, the effect of the alkaline reagent can be classified as follows: (i) thermal decomposition of the reagent, (ii) interaction with the oxidizing gas CO_2, (iii) interaction with constituents of the precursor, and (iv) catalyst of carbon gasification reactions.

With regard to the activation with NaOH, according to previous studies [55], the incorporated reagent can react with CO_2, giving way to the production of Na_2CO_3 (Eq. (9), which is then decomposed at high temperature, along with the remaining NaOH (Eqs. (10–11)). These gasification reactions involve the generation of porosity. As mentioned before, remarkable amounts of Na were detected in SCN samples (Table 2).

$$2\ NaOH\ (s,l) + CO_2\ (g) \rightarrow Na_2CO_3\ (s,l) + H_2O\ (g) \tag{9}$$

$$Na_2CO_3\ (s,l) \rightarrow Na_2O\ (s) + CO_2\ (g) \tag{10}$$

$$2\ NaOH\ (s,l) \rightarrow Na_2O\ (s) + H_2O\ (g) \tag{11}$$

Furthermore, according to the mechanism proposed by Zou et al. [55], NaOH and Na_2O can react with SiO_2 inorganic constituent of the precursor (Table 2), as shown in Eqs. (12)–(13). This reaction set does not imply gasification reactions and, consequently, does not contribute to the generation of porosity.

$$2\ NaOH\ (s) + SiO_2\ (s) \rightarrow Na_2SiO_3\ (s) + H_2O\ (l) \tag{12}$$

$$Na_2O\ (s) + SiO_2\ (s) \rightarrow Na_2SiO_3\ (s) \tag{13}$$

The impregnation with K_2CO_3 would contribute to the development of porosity through a similar mechanism. Apart from the thermal decomposition of K_2CO_3 (Eq. (15), the transformation of carbonates into OH^- ions in the presence of water (Eq. (14) has been reported [51, 56]. KOH would then be decomposed at high temperature (Eq. (16). The results of XRF (Table 2) evidence the presence of important amounts of K in SCK samples.

$$K_2CO_3\ (s,l) + H_2O\ (g) \rightarrow 2\ KOH\ (s,l) + CO_2\ (g) \tag{14}$$

$$K_2CO_3\ (s,l) \rightarrow K_2O\ (s) + CO_2\ (g) \tag{15}$$

$$2\ KOH\ (s,l) \rightarrow K_2O\ (s) + H_2O\ (g) \tag{16}$$

Furthermore, the treatment with NaOH incorporates OH^- ions, thus resulting in a greater extent of the reactions between carbon and OH^- ions (Eqs. (7) and (8)). These reactions involve the gasification of sludge constituents and, in addition, would lead to the production of carbonates, which would then be decomposed at high temperature, thus enhancing the generation of pores. The formation

of OH^- ions through Eq. (14) upon the impregnation with K_2CO_3 would have the same effect (Fig. 2).

The impregnation would also enhance the gasification of carbon. Indeed, the catalytic role of K and Na metals is well known for both the reverse Boudouard reaction (Eq. (4), and the gasification of carbon with steam (Eq. (5), being K the most active [57, 58].

As discussed below (Sect. 3.3.4., Fig. 3), the alkali activation promotes the generation of magnetite (Fe_3O_4), absent in samples of biochar prepared by physical activation only. The high iron content of the prepared materials (Table 2) reflects the addition of iron-containing coagulants such as PFC (polyferric chloride) or PFS (polyferric sulfate), during the wastewater treatment [59].

Two possible mechanisms are proposed for the generation of magnetite. The first one (Eq. (17) implies the direct formation of Fe_3O_4 from the reaction of Fe^{3+} with hydroxides. The second mechanism (Eqs. (18)–(19) involves the generation of $Fe(OH)_3$ and its subsequent transformation into magnetite, following a scheme similar to that proposed by Tang et al. [59] for the formation of Fe_2O_3:

$$3\ Fe^{3+} + 8\ OH^- + e^- \rightarrow Fe_3O_4 + 4\ H_2O \quad (17)$$

$$Fe^{3+} + 3\ OH^- \rightarrow Fe(OH)_3 \quad (18)$$

$$3\ Fe(OH)_3 + e^- \rightarrow Fe_3O_4 + 4\ H_2O + OH^- \quad (19)$$

The effect of the addition of the alkali reagent is clear in both reaction mechanisms. The treatment with NaOH directly incorporates OH^- ions, whereas the impregnation with K_2CO_3 would have the same effect, as a result of the generation of OH^- ions through Eq. (14).

3.2 Sludge carbon yield and ash content

The results of ash content and partial and overall yields are listed in Table 3. The impregnation yield (Y_{impr}) was calculated as the ratio between the weight of the sample after and before the impregnation with K_2CO_3 and NaOH. It is noteworthy that the impregnation with K_2CO_3 results in an increase in mass, due to the partial retention of the salt. On the contrary, the treatment with NaOH leads to a decrease in mass, suggesting an interaction between the reagent and the structure.

The yield of the activation step with CO_2 (Y_{CO2}, on a dry basis) was obtained from the mass of the sample prior and after treatment with CO_2. The overall yield of sludge carbon (Y_{SC}) was calculated as the product of the individual yields. As expected, Y_{CO2} decreases with temperature, whereas the ash content is increased. These results could be explained by the decomposition/volatilization or gasification of sludge constituents and/or incorporated species at high temperature, thus leading to the concentration of the mineral constituents. It is noteworthy that Y_{CO2} is higher for the samples impregnated with K_2CO_3 and NaOH, compared to non-impregnated samples. Moreover, the highest overall yield corresponds to the samples activated with K_2CO_3. As commented before, this result could be attributed to the high amount of salts incorporated during the impregnation (Table 2).

Table 3 Overall carbon yield and partial yields of different preparation steps (impregnation, activation with CO_2), ash content, and pH

Sample	Y_{impr} (wt%)	Y_{CO2} (wt%)	Y_{SC} (wt%)	Ash content (wt%)	pH
Raw sludge	–	–	–	42.2	7.2
SC-600	–	60.5	60.5	64.4	7.4
SC-700	–	57.7	57.7	67.3	7.5
SC-800	–	52.1	52.1	76.2	7.5
SC-900	–	42.2	42.2	92.2	7.7
SC-1000	–	38.7	38.7	99.8	7.7
SCK-600	120.0	71.2	85.4	64.7	9.4
SCK-700	120.0	64.0	76.8	78.7	9.6
SCK-800	120.0	56.6	67.9	82.1	9.8
SCK-900	120.0	52.2	62.6	85.7	10.3
SCK-1000	120.0	51.7	62.0	n.a	10.4
SCN-600	42.5	79.4	33.7	73.7	9.9
SCN-700	42.5	65.2	27.7	88.4	10.2
SCN-800	42.5	58.9	25.0	94.5	10.1
SCN-900	42.5	55.8	23.7	95.9	10.2
SCN-1000	42.5	54.4	23.1	n.a	10.2

n.a. Not analyzed

3.3 Characterization of sludge biochars

3.3.1 Textural properties

Table 4 summarizes the textural properties of the materials, and Fig. 2 shows the results of pore size distribution (PSD) of sludge biochar, measured by the BJH method. The materials possess a hierarchical structure, with a multimodal pore-size distribution (peaks at around 20, 80–100, and 300–500 Å).

Concerning the samples prepared by activation with CO_2 only (SC), the temperature that provides the highest value of specific surface area (S_{BET} of 113 m^2/g) and pore volume (0.156 cm^3/g) is 800 °C. The maximum value of micro- and mesoporosity (40.7 and 44.0 m^2/g, respectively) is also obtained at this temperature. For SC-800, the main contribution to specific surface area comes from pores up to 80 Å, for which the effect of temperature is especially strong. Lower temperatures are not effective to develop porosity, in good agreement with other authors [23, 37], who state that high temperatures are required for the activation with CO_2 to be effective. Temperatures higher than 900 °C have

Table 4 Textural properties of the prepared samples of sludge carbon. S m^2/g; V cm^3/g, D_p, Å

	S_{BET}	S_{micro} [a]	S_{meso} [b]	S_{macro} [b]	V_{micro} [a]	V_{meso} [b]	V_{macro} [b]	V_{total} [c]	D_p [d]
SC-600	58.4	15.0	34.3	2.1	0.0063	0.0885	0.0489	0.144	78.4
SC-700	50.7	11.5	30.8	3.9	0.0048	0.0825	0.0554	0.143	84.1
SC-800	113	40.7	44.0	0.8	0.0178	0.0923	0.0462	0.156	50.5
SC-900	43.1	3.5	29.9	2.5	0.0013	0.0693	0.0707	0.141	84.7
SC-1000	3.5	0.6	0.4	0.1	0.00006	0.0009	0.0021	0.003	28.9
SCK-600	129	74.4	38.0	2.3	0.0325	0.0915	0.0527	0.177	47.3
SCK-700	154	62.1	51.3	5.5	0.0270	0.1103	0.1490	0.286	48.3
SCK-800	41.2	13.9	13.2	8.5	0.0058	0.0651	0.2203	0.291	105
SCK-900	35.6	2.5	33.2	1.6	0.0011	0.0854	0.0335	0.120	112
SCN-600	93.3	35.8	41.0	3.5	0.0157	0.1034	0.0769	0.196	65.3
SCN-700	47.3	11.3	30.9	2.5	0.0049	0.0980	0.0654	0.168	103
SCN-800	9.7	2.0	1.2	4.6	0.0007	0.0057	0.1162	0.123	192
SCN-900	11.1	0.4	6.7	2.8	0.00007	0.0314	0.0635	0.095	165

[a]t-plot method

[b]BJH method (adsorption branch)

[c]Sum of t-plot and BJH methods

[d]BET method

a detrimental effect. The destructive effect of the activation temperature of 1000 °C is noteworthy in the whole pore range (Fig. 2), due to pore deformation, cracking, or blockage [60].

Regarding the impregnation with K_2CO_3, lower temperatures are required to achieve suitable textural properties. The highest value of S_{BET} (154 m^2/g) is obtained at 700 °C. This value is slightly higher than that obtained at 600 °C (129 m^2/g). SCK-700 exhibits the highest mesoporosity (51.3 m^2/g and 0.1103 cm^3/g) of the samples activated with K_2CO_3, which is mainly due to pores up to 100 Å (Fig. 2) whereas SCK-600 possesses the highest microporosity (74.4 m^2/g and 0.0325 cm^3/g), which represents around fivefold increase as compared to non-chemically treated sample (SC-600). An increasing temperature has the effect of decreasing microporosity, the effect being noteworthy above 800 °C. The highest total pore volume corresponds to SCK-700 and SCK-800 (0.286 and 0.291 cm^3/g, respectively). In the case of the sample activated at 800 °C, this high value of porosity is mainly due to its high degree of macroporosity. The different pore size distribution of SCK-800 and SCK-900 should be highlighted. The sample activated at 800 °C exhibits a dramatic decrease in mesopores up to 100 Å (compared to samples activated at lower temperature), and an important increase in pores higher than 500 Å (large mesopores and macropores), likely due to pore cracking. Contrary to expected, further increase in temperature (from 800 to 900 °C) gives way to a rise in mesoporosity especially in the 40–100 Å range. This phenomenon should be attributed to the occurrence of reactions or processes at high temperature involving the activating agent (such as the aforementioned thermal decomposition of K_2CO_3) that results in the development of porosity.

Compared to samples subjected to physical activation only, at temperatures up to 700 °C, the use of K_2CO_3 leads to an outstanding increase in S_{BET} (129 vs. 58.4 m^2/g at 600 °C; 154 vs. 50.7 m^2/g at 700 °C) and microporosity (74.4 vs. 15.0 m^2/g, and 62.1 vs. 11.5 m^2/g, respectively). On the contrary, at higher temperatures the treatment with K_2CO_3 has a detrimental effect on the development of porosity, the highest difference being obtained at 800 °C (S_{BET} = 41.2 and 113 m^2/g and S_{micro} = 13.9 and 40.7 m^2/g, for SCK-800 and SC-800, respectively).

The impregnation with NaOH prior to the activation with CO_2 results also in a trimodal PSD, though with a higher development of pores larger than 100 Å, compared to SC samples. Among the temperatures studied, the most suitable is 600 °C, since it provides the best textural properties: S_{BET} (93.3 m^2/g), microporosity (35.8 m^2/g), mesoporosity (41.0 m^2/g), and V_{total} (0.196 cm^3/g). These values are better than those obtained at 600 °C using physical activation only (59.8% of increase in S_{BET} and 139% in S_{micro}), but do not improve those obtained using K_2CO_3. Note that similar textural properties are attained without impregnation by a more severe thermal treatment, at around 800 °C. It is noteworthy that the same phenomenon observed for SCK samples takes place, evidenced by the different PSD of SCN-800 and SCN-900. Whereas the activation at 800 °C (SCN-800) causes a drastic decrease in mesopores up to 100 Å, with most of its specific area in large mesopores and macropores (possibly due to pore cracking, the average pore diameter being 192 Å);, further increase in temperature (900 °C) better preserves mesoporosity, up to 300 Å. This phenomenon could be related to the effect of the activating agent, noteworthy at high temperatures. As proposed for SCK samples, the

reactions which generate carbonates, along with the subsequent thermal decomposition, could explain the generation of new porosity.

Excessive activation temperatures have an important detrimental effect on porosity (micro- and mesoporosity, mainly up to 80 Å), and the optimum value depends on the chemical treatment. For instance, the optimum values of specific surface area and pore volume are obtained at 800 °C for SC, 700 °C for SCK, and 600 °C for SCN samples.

3.3.2 SEM

SEM analysis (Figure S1 given in Online Resource 1) reveals that a temperature of 800 °C causes the most prominent modification of the surface morphology of non-impregnated samples of sludge biochar (SC), in line with the abovementioned trend in BET and pore volume data. Moreover, as will be discussed in Sect. 3.4, these features definitely enable an easy access for methylene blue and phenol molecules and also contribute to the adsorption on surface. Figure S2 (Online Resource 1) shows the SEM images of selected samples of biochars prepared through chemical impregnation prior to the activation with CO_2 at 800 °C. The treatment with NaOH smooths the surface and causes a significant loss of BET area and pore volume (mainly micropore volume). The formation of tunnels and surface carvings upon the treatment with K_2CO_3 can be clearly observed. Such a significant alteration of the macropore structure is translated into an increased S_{macro} and V_{macro} for sample SCK-800 (Table 4), whereas specific surface area and total pore volume decrease.

3.3.3 EDX and XRF

Local EDX analyses (Table 5) reveal the high degree of heterogeneity of both the precursor (dried sewage sludge) and the prepared samples of biochar. Consequently, apart from the matrix, the composition of individual particles visible in surface has been determined.

The results show that in most cases the matrix is rich in oxygen, calcium, iron, silicon, phosphorus, and aluminum, in good agreement with the results of XRF (Table 2). As an exception, the sample activated at the highest temperature (SC-900) possesses a matrix rich in O, Fe, and Cr, and the other elements appear in hydroxyapatite-like individual particles.

The high amount of sulfur detected in many samples is noteworthy, either in the matrix or in individual particles, such as sulfates of Fe–Ca. These data reveal that S appears preferentially in the surface of biochars, given the low amount of sulfur detected by XRF (Table 2). Contrarily, the amount of Na measured is very low (with the exception of SC-900, in which Na was detected in the aforementioned individual particles), even in the sample impregnated with NaOH (SCN-800). The high amount of Na incorporated, detected by means of XRF (Table 2), evidences that this element is concentrated in the bulk of the material. Regarding the sample impregnated with K_2CO_3, important amounts of K are detected both in the matrix and in individual particles.

Apart from the aforementioned sulfates, other individual particles detected in biochars were identified as oxides or carbonates of Ca, phosphates of Fe–Ca, aluminosilicate-like

Table 5 Results of EDX analysis for selected samples of sludge biochar. Chemical composition of the prepared materials (wt%)

Sample	Analyzed area	O	Ca	Fe	P	S	Al	Si	Cr	Mn	Ni	K	Na	Observations
Precursor	Matrix	43.7	11.2	12.4	6.40	14.6	2.40	3.34	–	–	–	–	–	
	IP*	60.5	34.6	1.02	0.72	0.27	0.42	0.46	–	–	–	–	–	Oxides or carbonates of Ca
SC-600	Matrix	47.7	11.5	12.2	5.27	8.72	3.72	4.68	–	–	–	0.26	-	Hydroxyapatite-like
	IP1*	41.7	5.78	29.2	14.5	1.05	2.16	2.33	–	0.30	–	0.15	-	Phosphates of Fe–Ca
	IP2*	53.5	0.82	2.25	–	–	15.4	23.5	–	–	–	2.59	0.61	Aluminosilicate-like
SC-800	Matrix	36.6	16.2	17.6	10.8	2.49	6.59	5.88	–	–	–	0.50	–	
	IP1*	59.3	4.86	8.61	–	21.07	–	1.78	–	–	–	–	–	Sulfates of Fe–Ca
	IP2*	45.1	14.3	12.5	6.53	1.12	7.16	10.1	–	–	–	0.90	–	Aluminosilicate-like
SC-900	Matrix	35.1	0.30	29.2	0.44	0.14	0.20	0.42	27.4	1.89	2.91	–	0.65	
	IP1*	31.9	2.09	50.6	0.78	-	0.97	1.07	3.46	0.49	0.29	–	3.65	Iron oxides
	IP2*	47.7	9.28	12.1	5.66	0.14	5.97	9.26	1.17	–	–	0.45	6.68	Hydroxyapatite-like
SCK-800	Matrix	49.1	18.3	7.16	10.6	0.44	3.34	5.90	–	–	–	4.05	-	Hydroxyapatite-like
	IP1*	57.6	33.2	2.55	2.02	0.26	1.03	1.31	–	–	–	1.37	0.24	Oxides or carbonates of Ca
	IP2*	30.2	18.1	17.5	6.33	12.8	2.77	3.99	–	–	–	6.87	1.39	
SCN-800	Matrix	34.5	21.0	12.9	6.87	0.97	6.00	11.5	–	–	–	1.31	0.37	
	IP1*	42.3	0.45	0.40	–	–	–	54.9	–	–	–	–	–	Quartz
	IP2*	36.4	7.00	21.6	4.31	0.61	1.82	18.5	–	–	–	–	–	Iron oxides

*Individual particles visible in surface

aggregates, iron oxides, hydroxyapatite-like aggregates, and quartz (SiO_2).

3.3.4 XRD

XRD analyses were performed to investigate the crystalline structure. Strong and sharp reflection XRD peaks (Fig. 3) characteristic of SiO_2 are observed for all non-impregnated biochars. Also, calcite is observed for non-impregnated sludge carbons activated up to 800 °C (SC-600 to SC-800), whereas at the highest temperature (900 °C) it is absent. Moreover, at temperatures above 800 °C, sharp XRD peaks pertaining to more complex crystalline structures such as apatite ($Ca_5(PO_4)_3(OH)$) (PDF 9–432), $CaMgSi_2O_6$ (PDF 75–1092) and whitlockite ($Ca_{18,19}(Mg_{1.17}Fe_{0.83}H_{1.62}(PO_4)_{14})$) (PDF 70–1786) emerge as a result of the burning off of the volatile fraction.

In the case of the impregnated samples, the crystalline structure is significantly modified and new crystalline phases (i.e., magnetite, apatite) appear in sludge biochar even at the lowest temperature (600 °C). It is interesting to note that all the sludge carbons prepared by combined physical and chemical activation show magnetic properties, whereas the non-chemically treated samples do not contain magnetic particles (i.e., Fe_3O_4). It is interesting to note that the activation protocol used in this study is effective to generate biochar with magnetic properties through the transformation of the Fe introduced in the water treatment process into magnetite, without adding an iron source. The presence of magnetite is an advantage for the reuse of sewage sludge–based biochars in wastewater treatment, since it favors the removal of anionic surfactants [61] and heavy metals such as lead, copper, zinc, and manganese [62].

Also, in the impregnated samples, contrary to the non-impregnated SC samples, silicates are decomposed at high temperatures (i.e., no characteristic peaks of SiO_2 are detected in samples SCN-800, SCN-900, and SCK-900) and new and more complex crystalline phases are formed (Fig. 3b, c). The treatment with K_2CO_3 results in the formation of $KNO_3{\cdot}0.5H_2O$ (PDF 35–927) or $KAlSiO_4$ (PDF 33–988), as both phases have characteristic peaks in that range. Upon treatment with NaOH, new diffraction peaks emerge which can be ascribed to burkeite ($Na_6CO_3(SO_4)_2$) and hanksite ($Na_{22}K(CO_3)_2(SO_4)_9Cl$) phases. The appearance of new peaks upon the impregnation with either K_2CO_3 or NaOH supports the occurrence of reactions between the incorporated Na(II) and K(II) with sludge constituents.

3.3.5 Raman

Raman spectroscopy was performed to gain insight into the carbon structure. Figure 4 shows the Raman spectra of the precursor (raw sewage sludge) and selected samples of biochar. Regarding the precursor, a prominent photoluminescence background is observed, due to the incoherent vibrations of the high content of hydrogen [63]. The photoluminescence background is reduced when samples are subjected to pyrolysis, reflecting the reduction of the hydrogen content with an increasing degree of carbonization.

Except for SCN-800, every sample exhibits two peaks near 1360 and 1590 cm^{-1}, attributed to D and G bands, respectively. Generally, for highly ordered carbonaceous materials such as graphite or graphene, the D band indicates the presence of amorphous or disordered graphite, whereas the G band corresponds to graphitic crystallites [64]. Nevertheless, for highly disordered carbonaceous materials such as sewage sludge biochar, Li et al. [65] proposed that the D band should be more attributed to the breathing mode of sp^2-bonded carbon atoms in hexagonal aromatic rings, whereas the G band should be ascribed to bond stretching of all pairs of sp^2-bonded carbon atoms in both chains and rings. The D band is related to the structure disorder in the case of graphite, but for amorphous carbon, the development of the D band reveals structure ordering [66].

The ratio between the D and G bands can be used to determine the effect of the activation method on the carbonaceous structure of biochars. The deconvolution was necessary because of the large overlap between the D and G bands. Table S1 (Electronic Supplementary Material) provides the I_D/I_G and A_D/A_G ratios (corresponding to the intensity and area of the peaks, respectively). Both parameters follow the same trend. It is observed that the activation temperature has no visible effect on carbon structure, since the biochars prepared at 600–900 °C possess a similar I_D/I_G (0.91–0.94), slightly lower than that of the precursor (0.99). The chemical treatment, on the contrary, leads to an increase in the I_D/I_G

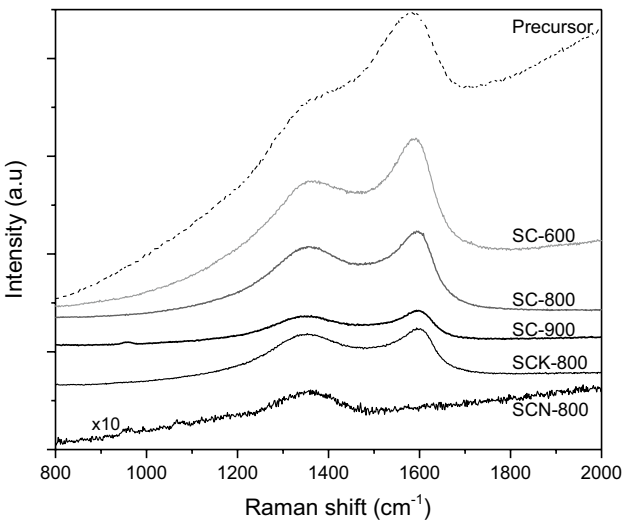

Fig. 4 Raman spectra of selected samples of sludge biochar

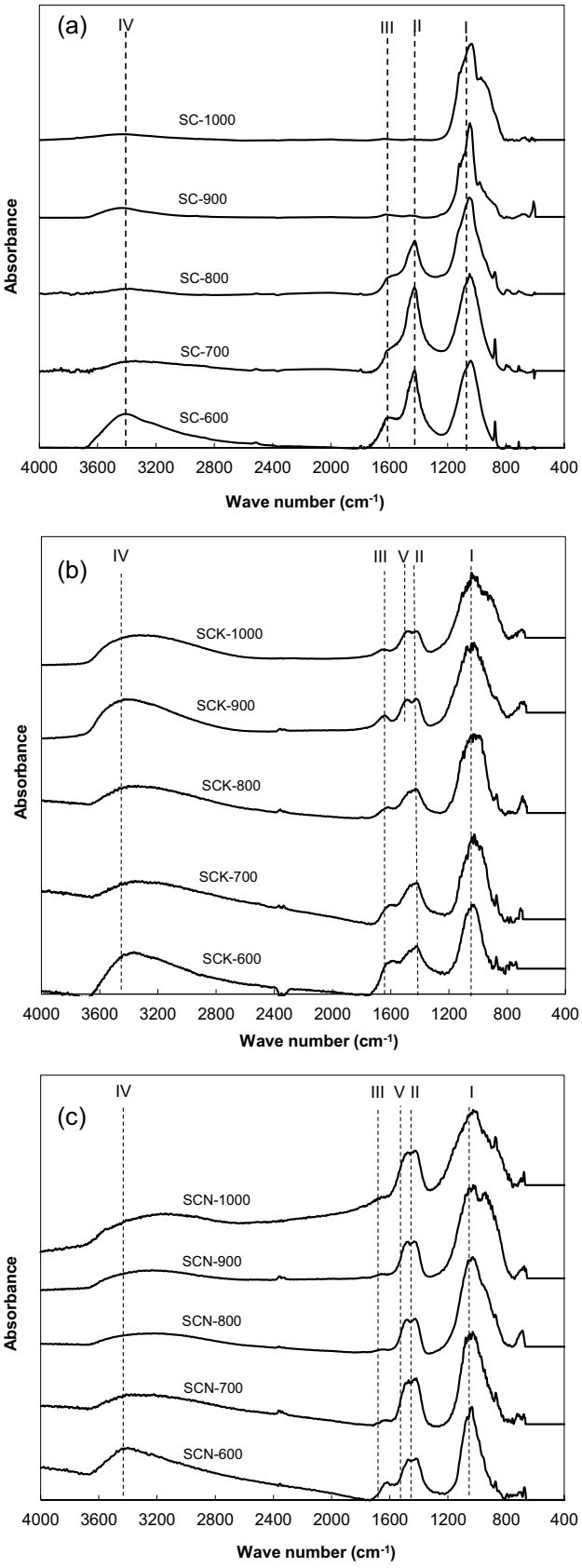

Fig. 5 FTIR spectra of samples of sludge carbon. **a** Samples prepared by physical activation with CO_2 only; **b** samples prepared by impregnation with K_2CO_3 followed by activation with CO_2; **c** samples prepared by impregnation with NaOH followed by activation with CO_2

ratio. This increase is moderate for K_2CO_3 (1.07 vs. 0.94), whereas for the sample activated with NaOH, only the D band is observed. Therefore, the chemical treatment results in the development of hexagonal aromatic rings and in the increase in the structural ordering of the carbon fraction.

3.3.6 FTIR

Figure 5 shows the FTIR spectra of all samples of biochar. Regarding the samples prepared by physical activation with CO_2 (Fig. 5a), the small peaks detected in the 600–750 cm^{-1} range, which do not show a clear trend with temperature, are attributed to the vibration of complex components of sludge carbon [55]. All materials exhibit a similar and predominant peak close to 1060 cm^{-1} (peak I), related to the silicon content. This band is indicative of structures such as Si–O–Si, Si–O–X (X = Al, Fe, Ca, Mg, and Na) and Si–O–C [25, 55]. The small peak observed at 870 cm^{-1} could also be attributed to Si–O–Si structure. The peak with its maximum near 1400 cm^{-1} (peak II) is difficult to assign. It could be ascribed to either organic sulfates, $CaCO_3$, or long-chain aliphatic structures (indicative of C–H bending band) [18]. This peak undergoes a dramatic decrease with temperature. Whereas a prominent and clearly defined peak is observed for SC-600, for SC-900 it almost disappears. This behavior can be ascribed to the decomposition of organic compounds and $CaCO_3$ at high temperature, in good agreement with the XRD results discussed above. The samples prepared between 600 and 800 °C also show a shoulder near 1600 cm^{-1} (peak III), which could be associated to carbonyl groups (C = O) [25, 67]. The intensity of this peak also decreases with temperature and above 900 °C it is almost completely absent. The broad band with its maximum close to 3400 cm^{-1} (peak IV) should be related to –OH and –NH surface functional groups [18, 19, 68], and could also be partially attributed to adsorbed water. This peak is strong for SC-600, and undergoes a drastic decrease above 700 °C.

Figure 5 b displays the FTIR spectra of the samples impregnated with K_2CO_3 followed by the activation with CO_2. In these spectra, the silicon content of the samples is still evident (band at 1060 cm^{-1}, peak I, which becomes broader with temperature). Regarding the peaks in the 1400–1600 cm^{-1} range, the treatment with K_2CO_3 results in important changes. The peak at 1400 cm^{-1} (peak II), attributed to calcite and long-chain aliphatic structures in SC samples, appears diminished for temperatures up to 800 °C, compared to SC samples, and a decreasing trend is observed in line with the characteristic XRD reflection peaks of calcite

in the SCK series. Taken into account that the impregnation step would result in an increase in the amount of carbonates, this result could be attributed to the enhancement of reactions that lead to the removal of aliphatic structures. For temperatures of 900–1000 °C, on the contrary, the size of this band remains almost constant, and two overlapping peaks (peaks II and V) can be distinguished (at lower activation temperature, a shoulder can be distinguished), suggesting the presence of new functionalities. Several authors [68–70] attributed a band near 1450 cm^{-1} to the presence of the C = C bond of aromatic rings polarized by oxygen atoms bound near one of the C atoms, suggesting the presence of basic oxygen-containing functionalities, such as chromene structures, diketones of quinone groups, and pyrone-like groups. The peak near 1490 cm^{-1} (peak V) might also signal the presence of nitrogen-containing groups, as reported in sludge-derived carbons prepared at high temperature (above 800 °C) [24, 71]. This phenomenon, that is, the occurrence of reactions and/or processes at high temperature level for samples impregnated with K_2CO_3, is in good agreement with the results of textural properties. As mentioned before, when the activation temperature is increased from 800 to 900 °C, there is an important increase in mesoporosity.

Regarding the band at 1600 cm^{-1} (peak III), related to C = O functionalities, it still appears as a shoulder. This peak shows a decreasing trend with temperature, as occurred for SC samples, but still can be distinguished at high temperatures (above 900 °C). The impregnation with K_2CO_3 has also the effect of increasing –OH and –NH functional groups (broad peak with its maximum close to 3400 cm^{-1}, peak IV). This peak is maximum for the lowest temperature studied (600 °C), as occurred for SC samples. However, the decrease with temperature is less pronounced for SCK samples. In fact, SCK-900 and SCK-1000 still exhibit an appreciable peak, higher than that of SCK-700 and SCK-800, thus suggesting the occurrence of mechanisms that involve the generation of those functionalities, such as Eq. (14).

The FTIR spectra of the samples prepared by impregnation with NaOH followed by activation with CO_2 are shown in Fig. 5c. As occurred with SC and SCK samples, the high intensity of peak I is related to the silicon content of the materials. Note that strong XRD diffraction peaks in SCN-800 and SCN-900, ascribed to $Na_2O{\cdot}Al_2O_3{\cdot}SiO_2$, can be observed. The most visible effect of the impregnation with NaOH is in the 1300–1500 cm^{-1} range. As occurred with SCK samples at high temperatures, two overlapping bands can be distinguished (peaks II and V), suggesting the occurrence of reactions that involve the generation of oxygen- and nitrogen-containing functionalities. These peaks are more pronounced than those obtained after the impregnation with K_2CO_3. Furthermore, they do not exhibit important variations with temperature. The peak of C = O (near 1600 cm^{-1}) appears as a shoulder (peak III), as in SC and SCK samples. This peak exhibits its maximum at the lowest activation temperature studied (600 °C), and is lower than that of SC-600 sample. The amount of C = O groups decreases with temperature. Concerning the effect of the impregnation with NaOH on the amount of –OH and –NH surface functional groups (broad peak close to 3400 cm^{-1}, peak IV), it is qualitatively similar but less pronounced than that of the impregnation with K_2CO_3. That is, the peak is maximum for the activation temperature of 600 °C, and the decrease with temperature is lower than for SC samples, the peak still being appreciable at 900 and 1000 °C.

3.3.7 pH

Table 3 shows the pH values of the prepared materials. The samples prepared by physical activation with CO_2 are slightly basic in nature, in good agreement with the results reported in the literature [4], with values of pH ranging from 7.4 to 7.7. The impregnation with either K_2CO_3 or NaOH results in an increase of the pH, with values in the 9.4–10.4 range for SCK samples, and 9.9–10.2 for SCN samples. In all cases, the pH increases with the activation temperature, which can be attributed to the decomposition and/or desorption of acidic functional groups (C = O and –OH and –NH) [27, 72], as confirmed by FTIR analyses (Fig. 5). Moreover, the increase in the basic character of sludge biochar as a result of the impregnation with K_2CO_3 and NaOH is in line with the generation of basic oxygen-containing functionalities observed in the FTIR spectra.

3.4 Adsorption of methylene blue and phenol

The adsorption isotherms of methylene blue and phenol at 20 °C for the prepared materials are shown in Figures S3 and S4 (given in Online Resource 1).

Table 6 summarizes the adsorption capacity of each material, as well as the parameters of best fit for the Redlich-Peterson model.

Among the samples prepared by physical activation only, the highest adsorption capacity of both MB and phenol (30.2 and 13.5 mg/g, respectively) corresponds to SC-800. This sample has the highest values of S_{BET}, V_{micro}, V_{meso}, and V_{total}. Regarding the materials prepared by impregnation with K_2CO_3 followed by activation with CO_2, SCK-700 exhibits the highest removal ability of MB (56.1 mg/g) and phenol (25.3 mg/g). These values represent an increase of 87%, compared to the best value of SC samples, and in the case of MB, it is the highest value of all samples. The high adsorption capacity of SCK-700 could be explained by its suitable textural properties. This sample has the highest values of S_{BET} and V_{meso} and 98% of the highest V_{micro}, along with a suitable surface chemistry—second highest band of carbonyl groups among SCK samples, which has been

Table 6 Best fit Redlich-Peterson isotherm parameters for MB and phenol adsorption and experimental uptake of both adsorbates

	Adsorption of MB					Adsorption of phenol				
	q_{exp}, mg/g	K_R, L/g	α (L/mg)$^{\beta}$	β	APE	q_{exp}, mg/g	K_R, L/g	α (L/mg)$^{\beta}$	β	APE
SC-600	20.6	5.04	0.262	0.973	0.54	10.0	0.318	0.036	0.956	0.92
SC-700	16.1	5.28	0.514	0.892	2.03	8.9	0.287	0.028	1.000	5.20
SC-800	30.2	17.4	0.832	0.908	3.60	13.5	0.847	0.058	1.000	2.78
SC-900	16.5	40.6	3.609	0.909	3.72	6.5	0.283	0.069	0.897	1.18
SC-1000	5.9	0.41	0.059	0.998	0.69	3.1	0.123	0.038	0.988	1.20
SCK-600	52.8	64.6	2.219	0.862	0.64	17.5	0.42	0.034	0.914	1.18
SCK-700	56.1	72.7	1.898	0.916	1.38	25.3	1.68	0.183	0.810	0.73
SCK-800	31.2	170.9	20.9	0.700	2.42	21.2	0.51	0.049	0.843	1.84
SCK-900	12.1	0.38	0.020	1.000	2.16	8.4	0.82	0.387	0.746	0.37
SCN-600	35.0	12.2	0.440	0.943	0.29	34.0	0.61	0.031	0.871	1.77
SCN-700	30.3	3.29	0.095	1.000	1.62	18.3	0.41	0.019	1.000	2.53
SCN-800	27.5	2.47	0.077	1.000	3.92	29.5	0.32	0.008	1.000	3.39
SCN-900	20.0	1.69	0.072	1.000	3.38	25.0	0.39	0.012	1.000	4.03

reported to favor the adsorption of MB [33]. Concerning the uptake of MB, the good value obtained with SCK-600 (52.8 mg/g) is noteworthy, only slightly lower than the maximum value. The latter has the advantage that a lower activation temperature is required. The good adsorption ability of SCK-600 could be explained by its good textural properties (S_{BET} and V_{meso} are lower than those of SCK-700, and V_{micro} is maximum) and suitable surface chemistry (the amount of C = O functionalities is the highest of SCK series). Activation temperatures above 700 °C have an important detrimental effect on the porosity, and thus, moderate temperatures are advisable for the activation with K_2CO_3.

Regarding the removal of phenol, the small difference between the adsorption capacity of both SCK-600 and SCK-800 (17.5 vs. 21.2 mg/g) is remarkable, given the great differences in the textural properties of both samples (S_{BET} = 129 m^2/g and S_{micro} = 74.4 m^2/g for SCK-600, and S_{BET} = 41.2 m^2/g and S_{micro} = 13.9 m^2/g for SCK-800). These results evidence that other factors, apart from textural properties, are implied in the adsorption process of phenol. It has been reported that phenol could be adsorbed not only by physisorption, but also by surface polymerization [73], favored by the presence of metals on the surface of the material. The much higher amount of ash of SCK-800, compared to SCK-600 (82.1 vs. 64.7 wt%), could then favor its phenol removal ability.

Among the materials prepared by impregnation with NaOH prior to activation with CO_2, the sample activated at 600 °C shows the highest MB and phenol removal ability (35.0 and 34.0 mg/g, respectively), the uptake capacity of phenol of SCN-600 being the highest of all the materials. This sample has the highest value of S_{BET}, V_{micro}, V_{meso}, V_{total}, and C = O functional groups among SCN samples. Compared to only physically activated samples, the maximum removal ability is increased by 15.9% (MB) and 152% (phenol), with the advantage that a mild activation is required (600 °C for SCN samples vs. 800 °C for SC).

Regarding the adsorption of MB of SCN samples, temperatures higher than 600 °C result in a decrease, which could be attributed to the decrease in S_{BET}, V_{meso}, and V_{total} (Table 4) and carbonyl groups (Fig. 5). Concerning the adsorption of phenol, the good uptake capacity of all SCN materials is noteworthy, even for the materials prepared at high temperature. This result could be attributed to the aforementioned generation of new functionalities containing oxygen and/or nitrogen as a consequence of the chemical activation with NaOH (Fig. 5c, peak V), in good agreement with the results reported in the literature [74] for the adsorption of phenolic compounds. The size of the peak is similar for all activation temperatures and thus, it would result in a good adsorption capacity of phenol within the whole temperature range studied. The aforementioned hypothesis that phenol could also be adsorbed by surface polymerization, favored by the presence of metals on the surface of the material (their amount increasing with temperature, Table 3), also contributes to explain the high uptake capacity of SCN samples activated at high temperatures. The removal ability of phenol decreases with temperature, which is in good agreement with the decreasing trend with temperature of the microporosity as shown in Table 4.

4 Conclusions

The proposed activation mechanism of non-impregnated sludge includes (i) the decomposition/volatilization of organic and inorganic constituents; (ii) the desorption of water; (iii) the gasification of carbon; and (iv) the reaction

of carbon and OH^- to produce compounds such as cyanides, hydrocarbons, and carbonates. The impregnation with K_2CO_3 or NaOH would lead to (i) the thermal decomposition of carbonates and hydroxides, directly incorporated or formed from the reagent; (ii) the intensification of the set of reactions between carbon and OH^-, due to the incorporated or generated OH^- ions; (iii) the enhancement of carbon gasification, owing to the catalytic role of K and Na; and (iv) the generation of magnetite (Fe_3O_4) from the reaction of Fe^{3+} with hydroxides.

From the standpoint of textural properties, the impregnation results in a decrease in the optimum activation temperature: 800 °C for untreated (SC) samples, and 600–700 °C for the samples impregnated with K_2CO_3 (SCK) and NaOH (SCN). The highest value of S_{BET} of all samples corresponds to SCK-700 (increase of 36% compared to SC-800), whereas SCK-600 possesses a slightly lower value, along with the highest microporosity (83% of increase vs. SC-800). The impregnation increases the amount of surface –OH and –NH functional groups, also detected in non-impregnated biochars, the effect being more pronounced for K_2CO_3. It also results in the generation of new functionalities (in the whole temperature range for NaOH and above 800 °C for K_2CO_3), attributed to oxygen and/or nitrogen containing groups.

SCK-700 has the highest MB removal ability, whereas SCK-600 exhibits an only slightly lower adsorption capacity. These samples combine suitable textural properties and surface chemistry (high amount of carbonyl groups). SCN-600 possesses the highest phenol adsorption capacity. The optimum uptake values represent an increase of 87% and 152% for MB and phenol, respectively, compared to the highest value of non-impregnated samples (SC-800), with the advantage of the lower temperature required. The good phenol uptake capacity of all SCN samples could be attributed to (i) the generation of the new functionalities containing nitrogen and/or oxygen and (ii) the adsorption of phenol by surface polymerization.

The chemical treatment develops magnetic properties in biochar, an advantage for its reuse in wastewater treatment, since it favors the removal of anionic surfactants and heavy metals such as lead, copper, zinc, and manganese.

Supplementary Information The online version contains supplementary material available at https://doi.org/10.1007/s13399-022-02372-w.

Acknowledgements The authors are grateful for the technical and human support provided by SCAB and SCAA (SGIker) of UPV/EHU and European funding (ERDF and ESF).

Funding Open Access funding provided thanks to the CRUE-CSIC agreement with Springer Nature. This work was supported by the Basque Government (UFI 11/39 (UPV/EHU) and S-PE13UN100 project).

Declarations

Ethics approval Not applicable.

Consent to participate Not applicable.

Consent for publication Not applicable.

Competing interests The authors declare no competing interests.

References

1. Racek J, Sevcik J, Chorazy T, Kucerik J, Hlavinek P (2020) Biochar - recovery material from pyrolysis of sewage sludge: a review. Waste Biomass Valor 11:3677–3709. https://doi.org/10.1007/s12649-019-00679-w
2. Wang J, Wang S (2019) Preparation, modification and environmental application of biochar: a review. J Clean Prod 227:1002–1022. https://doi.org/10.1016/j.jclepro.2019.04.282
3. Rorat A, Courtois P, Vandenbulcke F, Lemiere S (2019) 8 - sanitary and environmental aspects of sewage sludge management. In: Prasad MNV, De Campos Favas PJ, Vithanage M, Mohan SV (eds) Industrial and Municipal Sludge. Butterworth-Heinemann, Oxford, pp 155–180. https://doi.org/10.1016/B978-0-12-815907-1.00008-8
4. Smith KM, Fowler GD, Pullket S, Graham NJD (2009) Sewage sludge-based adsorbents: a review of their production, properties and use in water treatment applications. Water Res 43(10):2569–2594. https://doi.org/10.1016/j.watres.2009.02.038
5. Tu W, Liu Y, Xie Z, Chen M, Ma L, Du G, Zhu M (2021) A novel activation-hydrochar via hydrothermal carbonization and KOH activation of sewage sludge and coconut shell for biomass wastes: preparation, characterization and adsorption properties. J Colloid Interf Sci 593:390–407. https://doi.org/10.1016/j.jcis.2021.02.133
6. Ma J, Zhou B, Zhang H, Zhang W (2020) Fe/S modified sludge-based biochar for tetracycline removal from water. Powder Technol 364:889–900. https://doi.org/10.1016/j.powtec.2019.10.107
7. Zhao B, Xu X, Zhang R, Cui M (2021) Remediation of Cu(II) and its adsorption mechanism in aqueous system by novel magnetic biochar derived from co-pyrolysis of sewage sludge and biomass. Environ Sci Pollut Res 28:16408–16419. https://doi.org/10.1007/s11356-020-11811-y

8. Li J, Yu G, Pan L, Li C, You F, Wang Y (2020) Ciprofloxacin adsorption by biochar derived from co-pyrolysis of sewage sludge and bamboo waste. Environ Sci Pollut Res 27:22806–22817. https://doi.org/10.1007/s11356-020-08333-y
9. Zhang J, Tian Y, Yin L, Zhang J, Drewes JE (2018) Insight into the effects of biochar as adsorbent and microwave receptor from one-step microwave pyrolysis of sewage sludge. Environ Sci Pollut Res 25:18424–18433. https://doi.org/10.1007/s11356-018-2028-9
10. Lin W, Gu H, Zhou J et al (2021) Calcium oxide-modified activated sludge as a low-cost biomass adsorbent for Cd(II) removal in aqueous solution: biosorption behavior and mechanism. Biomass Conv Bioref. https://doi.org/10.1007/s13399-021-01893-0
11. Fu C, Zhang L, Zhang K et al (2021) Effects of air-prepared atmosphere on the Pb^{2+} adsorption of sludge-based adsorbent. Biomass Conv Bioref. https://doi.org/10.1007/s13399-021-01706-4
12. Singh S, Kumar V, Dhanjal DS, Datta S, Bhatia D, Dhiman J, Samuel J, Prasad R, Singh J (2020) A sustainable paradigm of sewage sludge biochar: valorization, opportunities, challenges and future prospects. J Clean Prod 269:122259. https://doi.org/10.1016/j.jclepro.2020.122259
13. Aliakbari Z, Younesi H, Ghoreyshi AA, Bahramifar N, Heidari A (2018) Production and characterization of sewage-sludge based activated carbons under different post-activation conditions. Waste Biomass Valor 9:451–463. https://doi.org/10.1007/s12649-016-9823-7
14. Hunsom M, Autthanit C (2013) Adsorptive purification of crude glycerol by sewage sludge-derived activated carbon prepared by chemical activation with H_3PO_4, K_2CO_3 and KOH. Chem Eng J 229:334–343. https://doi.org/10.1016/j.cej.2013.05.120
15. Sheha D, Khalaf H, Daghestani N (2013) Experimental design methodology for the preparation of activated carbon from sewage sludge by chemical activation process. Arab J Sci Eng 38:2941–2951. https://doi.org/10.1007/s13369-012-0470-4
16. Xi X, Guo X (2013) Preparation of bio-charcoal from sewage sludge and its performance on removal of Cr (VI) from aqueous solutions. J Mol Liq 183:26–30. https://doi.org/10.1016/j.molliq.2013.03.020
17. De Andrés JM, Orjales L, Narros A, De la Fuente MM, Rodríguez ME (2013) Carbon dioxide adsorption in chemically activated carbon from sewage sludge. J Air Waste Manag Assoc 63(5):557–564. https://doi.org/10.1080/10962247.2013.772927
18. Ros A, Montes-Moran M, Fuente E, Nevskaia DM, Martin MJ (2006) Dried sludges and sludge-based chars for H_2S removal at low temperature: influence of sewage sludge characteristics. Environ Sci Technol 40(1):302–309. https://doi.org/10.1021/es050996j
19. Khoshbouy R, Takahashi F, Yoshikawa K (2019) Preparation of high surface area sludge-based activated hydrochar via hydrothermal carbonization and application in the removal of basic dye. Environ Res 175:457–467. https://doi.org/10.1016/j.envres.2019.04.002
20. Zeng F, Liao X, Hu H, Liao L (2018) Effect of potassium hydroxide activation in the desulfurization process of activated carbon prepared by sewage sludge and corn straw. J Air Waste Manag Assoc 68(3):255–264. https://doi.org/10.1080/10962247.2017.1407378
21. Li Y, Li Y, Li L, Shi X, Wang Z (2016) Preparation and analysis of activated carbon from sewage sludge and corn stalk. Adv Powder Technol 27(2):684–691. https://doi.org/10.1016/j.apt.2016.02.029
22. Gupta A, Garg A (2015) Utilisation of sewage sludge derived adsorbents for the removal of recalcitrant compounds from wastewater: mechanistic aspects, isotherms, kinetics and thermodynamics. Bioresource Technol 194:214–224. https://doi.org/10.1016/j.biortech.2015.07.005
23. Xu G, Yang X, Spinosa L (2015) Development of sludge-based adsorbents: preparation, characterization, utilization and its feasibility assessment. J Environ Manag 151:221–232. https://doi.org/10.1016/j.jenvman.2014.08.001
24. Marques RRN, Stüber F, Smith KM, Fabregat A, Bengoa C, Font J, Fortuny A, Pullket S, Fowler GD, Graham NJD (2011) Sewage sludge based catalysts for catalytic wet air oxidation of phenol: preparation, characterisation and catalytic performance. Appl Catal B-Environ 101(3–4):306–316. https://doi.org/10.1016/j.apcatb.2010.09.033
25. Smith KM, Fowler GD, Pullket S, Graham NJD (2012) The production of attrition resistant, sewage–sludge derived, granular activated carbon. Sep Purif Technol 98:240–248. https://doi.org/10.1016/j.seppur.2012.07.026
26. Velghe I, Carleer R, Yperman J, Schreurs S, D'Haen J (2012) Characterisation of adsorbents prepared by pyrolysis of sludge and sludge/disposal filter cake mix. Water Res 46(8):2783–2794. https://doi.org/10.1016/j.watres.2012.02.034
27. Méndez A, Gascó G, Freitas MMA, Siebielec G, Stuczynski T, Figueiredo JL (2005) Preparation of carbon-based adsorbents from pyrolysis and air activation of sewage sludges. Chem Eng J 108(1–2):169–177. https://doi.org/10.1016/j.cej.2005.01.015
28. Sierra I, Iriarte-Velasco U, Cepeda EA, Gamero M, Aguayo AT (2016) Preparation of carbon-based adsorbents from the pyrolysis of sewage sludge with CO_2. Investigation of the acid washing procedure. Desalin Water Treat 57(34):16053–16065. https://doi.org/10.1080/19443994.2015.1075428
29. Alvarez J, Lopez G, Amutio M, Bilbao J, Olazar M (2016) Preparation of adsorbents from sewage sludge pyrolytic char by carbon dioxide activation. Process Saf Environ 103(A):76–86. https://doi.org/10.1016/j.psep.2016.06.035
30. Grifoni M, Pedron F, Rosellini I, Petruzzelli G (2019) From waste to resource: sorption properties of biological and industrial sludge. In: Prasad MNV, De Campos Favas PJ, Vithanage M, Mohan SV (eds) Industrial and Municipal Sludge. Butterworth-Heinemann, Oxford, pp 595–621. https://doi.org/10.1016/B978-0-12-815907-1.00026-X
31. Xiao Y, Raheem A, Ding L, Chen W, Chen X, Wang F, Lin S (2022) Pretreatment, modification and applications of sewage sludge-derived biochar for resource recovery- a review. Chemosphere 287(1):131969. https://doi.org/10.1016/j.chemosphere.2021.131969
32. Zhang J, Shao J, Jin Q, Zhang X, Yang H, Chen Y, Zhang S, Chen H (2020) Effect of deashing on activation process and lead adsorption capacities of sludge-based biochar. Sci Total Environ 716:137016. https://doi.org/10.1016/j.scitotenv.2020.137016
33. Sierra I, Iriarte-Velasco U, Gamero M, Aguayo AT (2017) Upgrading of sewage sludge by demineralization and physical activation with CO_2: application for methylene blue and phenol removal. Micropor Mesopor Mat 250:88–99. https://doi.org/10.1016/j.micromeso.2017.05.020
34. Kong L, Tian S, Luo R, Liu W, Tu Y, Xiong Y (2013) Demineralization of sludge-based adsorbent by post-washing for development of porosity and removal of dyes. J Chem Technol Biotechnol 88:1473–1480. https://doi.org/10.1002/jctb.3989
35. Paz-Ferreiro J, Nieto A, Méndez A, Askeland MP, Gascó G (2018) Biochar from biosolids pyrolysis: a review. Int J Environ Res Public Health 15(5):956. https://doi.org/10.3390/ijerph15050956
36. Martínez de Yuso A, Rubio B, Izquierdo MT (2014) Influence of activation atmosphere used in the chemical activation of almond shell on the characteristics and adsorption performance of activated carbons. Fuel Process Technol 119:74–80. https://doi.org/10.1016/j.fuproc.2013.10.024
37. Hadi P, Xu M, Ning C, Sze Ki Lin C, McKay G (2015) A critical review on preparation, characterization and utilization of sludge-derived activated carbons for wastewater treatment. Chem Eng J 260:895–906. https://doi.org/10.1016/j.cej.2014.08.088

38. Wang X, Zhu N, Yin B (2008) Preparation of sludge-based activated carbon and its application in dye wastewater treatment. J Hazard Mater 153(1–2):22–27. https://doi.org/10.1016/j.jhazmat.2007.08.011
39. Xiao X, Chen B, Chen Z, Zhu L, Schnoor JL (2018) Insight into multiple and multilevel structures of biochars and their potential environmental applications: a critical review. Environ Sci Technol 52:5027–5047. https://doi.org/10.1021/acs.est.7b06487
40. Xiao X, Chen Z, Chen B (2016) H/C atomic ratio as a smart linkage between pyrolytic temperatures, aromatic clusters and sorption properties of biochars derived from diverse precursory materials. Sci Rep 6:22644. https://doi.org/10.1038/srep22644
41. Chen Y, Wang R, Duan X, Wang S, Ren N, Ho S (2020) Production, properties, and catalytic applications of sludge derived biochar for environmental remediation. Water Res 187:116390. https://doi.org/10.1016/j.watres.2020.116390
42. Monsalvo VM, Mohedano AF, Rodriguez JJ (2011) Activated carbons from sewage sludge: application to aqueous-phase adsorption of 4-chlorophenol. Desalination 277(1–3):377–382. https://doi.org/10.1016/j.desal.2011.04.059
43. Kaçan E, Kütahyalı C (2012) Adsorption of strontium from aqueous solution using activated carbon produced from textile sewage sludges. J Anal Appl Pyrolysis 97:149–157. https://doi.org/10.1016/j.jaap.2012.06.006
44. Tessmer CH, Vidic RD, Uranowski LJ (1997) Impact of oxygen-containing surface functional groups on activated carbon adsorption of phenols. Environ Sci Technol 31(7):1872–1878. https://doi.org/10.1021/es960474r
45. Wang Z, Ma X, Yao Z, Yu Q, Wang Z, Lin Y (2018) Study of the pyrolysis of municipal sludge in N_2/CO_2 atmosphere. Appl Therm Eng 128:662–671. https://doi.org/10.1016/j.applthermaleng.2017.09.044
46. Xiaohua W, Jiancheng J (2012) Effect of heating rate on the municipal sewage sludge pyrolysis character. Energy Procedia 14:1648–1652. https://doi.org/10.1016/j.egypro.2011.12.1146
47. Li W, Yue Q, Gao B, Wang X, Qi Y, Zhao Y, Li Y (2011) Preparation of sludge-based activated carbon made from paper mill sewage sludge by steam activation for dye wastewater treatment. Desalination 278(1–3):179–185. https://doi.org/10.1016/j.desal.2011.05.020
48. Conesa JA, Marcilla A, Moral R, Moreno-Caselles J, Perez-Espinosa A (1998) Evolution of gases in the primary pyrolysis of different sewage sludges. Thermochim Acta 313(1):63–73. https://doi.org/10.1016/S0040-6031(97)00474-7
49. Nowicki L, Ledakowicz S (2014) Comprehensive characterization of thermal decomposition of sewage sludge by TG–MS. J Anal Appl Pyrol 110:220–228. https://doi.org/10.1016/j.jaap.2014.09.004
50. Zuo W, Jin B, Huang Y, Sun Y (2015) Thermal decomposition of three kinds of sludge by TG–MS and PY–GC/MS. J Therm Anal Calorim 121:1297–1307. https://doi.org/10.1007/s10973-015-4651-8
51. Iriarte-Velasco U, Ayastuy JL, Zudaire L, Sierra I (2014) An insight into the reactions occurring during the chemical activation of bone char. Chem Eng J 251:217–227. https://doi.org/10.1016/j.cej.2014.04.048
52. Robau-Sánchez A, Aguilar-Elguézabal A, Aguilar-Pliego J (2005) Chemical activation of Quercus agrifolia char using KOH: evidence of cyanide presence. Micropor Mesopor Mat 85(3):331–339. https://doi.org/10.1016/j.micromeso.2005.07.003
53. Lillo-Ródenas MA, Cazorla-Amorós D, Linares-Solano A (2003) Understanding chemical reactions between carbons and NaOH and KOH: an insight into the chemical activation mechanism. Carbon 41(2):267–275. https://doi.org/10.1016/S0008-6223(02)00279-8
54. Lillo-Ródenas MA, Juan-Juan J, Cazorla-Amorós D, Linares-Solano A (2004) About reactions occurring during chemical activation with hydroxides. Carbon 42(7):1371–1375. https://doi.org/10.1016/j.carbon.2004.01.008
55. Zou J, Dai Y, Wang X, Ren Z, Tian C, Pan K, Li S, Abuobeidah M, Fu H (2013) Structure and adsorption properties of sewage sludge-derived carbon with removal of inorganic impurities and high porosity. Bioresour Technol 142:209–217. https://doi.org/10.1016/j.biortech.2013.04.064
56. Yasukawa A, Kandori K, Ishikawa T (2003) TPD-TG-MS study of carbonate calcium hydroxyapatite particles. Calcif Tissue Int 72:243–250. https://doi.org/10.1007/s00223-002-2032-3
57. Ren H, Zhang Y, Fang Y, Wang Y (2011) Co-gasification behavior of meat and bone meal char and coal char. Fuel Process Technol 92(3):298–307. https://doi.org/10.1016/j.fuproc.2010.09.013
58. Acharya CK, Jiang F, Liao C, Fitzgerald P, Vecchio KS, Cattolica RJ (2013) Tar and CO_2 removal from simulated producer gas with activated carbon and charcoal. Fuel Process Technol 106:201–208. https://doi.org/10.1016/j.fuproc.2012.07.026
59. Tang L, Yu J, Pang Y, Zeng G, Deng Y, Wang J, Ren X, Ye S, Peng B, Feng H (2018) Sustainable efficient adsorbent: alkali-acid modified magnetic biochar derived from sewage sludge for aqueous organic contaminant removal. Chem Eng J 336:160–169. https://doi.org/10.1016/j.cej.2017.11.048
60. Mahapatra K, Ramteke DS, Paliwal LJ (2012) Production of activated carbon from sludge of food processing industry under controlled pyrolysis and its application for methylene blue removal. J Anal Appl Pyrol 95:79–86. https://doi.org/10.1016/j.jaap.2012.01.009
61. Makarchuk O, Dontsova T, Perekos A, Skoblik A, Svystunov Y (2017) Magnetic mineral nanocomposite sorbents for wastewater treatment. J Nanomater 2017:7. https://doi.org/10.1155/2017/8579598
62. Giraldo L, Erto A, Moreno-Piraján JC (2013) Magnetite nanoparticles for removal of heavy metals from aqueous solutions: synthesis and characterization. Adsorption 19:465–474. https://doi.org/10.1007/s10450-012-9468-1
63. Tsaneva VN, Kwapinski W, Teng X, Glowacki BA (2014) Assessment of the structural evolution of carbons from microwave plasma natural gas reforming and biomass pyrolysis using Raman spectroscopy. Carbon 80:617–628. https://doi.org/10.1016/j.carbon.2014.09.005
64. Zhang J, Lü F, Zhang H, Shao L, Chen D, He P (2015) Multiscale visualization of the structural and characteristic changes of sewage sludge biochar oriented towards potential agronomic and environmental implication. Sci Rep 5:9406. https://doi.org/10.1038/srep09406
65. Li M, Tang Y, Ren N, Zhang Z, Cao Y (2018) Effect of mineral constituents on temperature-dependent structural characterization of carbon fractions in sewage sludge-derived biochar. J Clean Prod 172:3342–3350. https://doi.org/10.1016/j.jclepro.2017.11.090
66. Ferrari A, Robertson J (2000) Interpretation of Raman spectra of disordered and amorphous carbon. Phys Rev B 61:14095–14107. https://doi.org/10.1103/PhysRevB.61.14095
67. Shi L, Zhang G, Wei D, Yan T, Xue X, Shi S, Wei Q (2014) Preparation and utilization of anaerobic granular sludge-based biochar for the adsorption of methylene blue from aqueous solutions. J Mol Liq 198:334–340. https://doi.org/10.1016/j.molliq.2014.07.023
68. Jindarom C, Meeyoo V, Kitiyanan B, Rirksomboon T, Rangsunvigit P (2007) Surface characterization and dye adsorptive capacities of char obtained from pyrolysis/gasification of sewage sludge. Chem Eng J 133(1–3):239–246. https://doi.org/10.1016/j.cej.2007.02.002
69. Martin MJ, Artola A, Balaguer MD, Rigola M (2003) Activated carbons developed from surplus sewage sludge for the removal of

dyes from dilute aqueous solutions. Chem Eng J 94(3):231–239. https://doi.org/10.1016/S1385-8947(03)00054-8
70. Fuente E, Menendez JA, Suarez D, Montes-Moran MA (2003) Basic surface oxides on carbon materials: a global view. Langmuir 19(8):3505–3511. https://doi.org/10.1021/la026778a
71. Bandosz TJ, Block K (2006) Effect of pyrolysis temperature and time on catalytic performance of sewage sludge/industrial sludge-based composite adsorbents. Appl Catal B-Environ 67(1–2):77–85. https://doi.org/10.1016/j.apcatb.2006.04.006
72. Hofman M, Pietrzak R (2012) NO_2 removal by adsorbents prepared from waste paper sludge. Chem Eng J 183:278–283. https://doi.org/10.1016/j.cej.2011.12.077
73. Leng C-C, Pinto NG (1997) Effects of surface properties of activated carbons on adsorption behavior of selected aromatics. Carbon 35(9):1375–1385. https://doi.org/10.1016/S0008-6223(97)00091-2
74. Lin S, Juang R (2009) Adsorption of phenol and its derivatives from water using synthetic resins and low-cost natural adsorbents: a review. J Environ Manag 90(3):1336–1349. https://doi.org/10.1016/j.jenvman.2008.09.003